3D-printed ceramics with engineered anisotropy for dielectric resonator antenna applications

C. D. Morales [1] ✉, C. Morlaas, [1] A. Chabory, [1] R. Pascaud, [2] M. Grzeskowiak, [2] and G. Mazingue [3]

[1] *ENAC, Université de Toulouse, Toulouse, France*

[2] *ISAE-SUPAERO, Université de Toulouse, Toulouse, France*

[3] *ANYWAVES, Toulouse, France*

✉ Email: carlosdavid.moralespena@enac.fr

In this letter, we study the design of three-dimensional (3D)-printed ceramics exhibiting anisotropic dielectric permittivities at microwave frequencies for dielectric resonator antenna (DRA) applications. The anisotropy is engineered by using periodic structures made up of sub-wavelength asymmetric unit cells filled with zirconia and air. Ceramic samples with uniaxial anisotropy are designed, 3D-printed, and measured. Birefringence up to 8 is achieved by controlling the volume fill rate of the unit cell. Besides, a single-fed circularly polarised (CP) DRA that relies on a 3-D-printed uniaxial anisotropic ceramic is proposed in the 2.45 GHz ISM band. Its simulated and measured reflection coefficient, axial ratio, and realised gain patterns are in good agreement, thus demonstrating the possibility of exploiting 3-D-printed anisotropic ceramics for DRA applications.

Introduction: The dielectric resonator antenna (DRA) has been extensively studied to take advantage of it's reduced size, ease of excitation, high radiation efficiency and wide bandwidth [1]. It allows great flexibility in its design by modifying its shape or dielectric properties to control, for instance, its impedance bandwidth or radiation characteristics.

If the fabrication of heterogeneous DRAs with complex shapes has so far been limited by traditional manufacturing methods such as tooling, machining, or moulding, recent advances in three-dimensional (3D)-printing technologies are opening up new perspectives. Complex shapes have thus been achieved such as super-shaped DRAs based on photopolymer stereolithography apparatus (SLA) [2], or even full DRA reflectarrays manufactured using the fused deposition modelling (FDM) printing technique [3]. It has also been proposed to control the effective permittivity of DRAs by structuring the 3D-printed material. In that case, subwavelength unit cells consisting of both air and dielectric are periodically 3D-printed so as to obtain a material which effective dielectric permittivity is controlled by the volume fill rate of its unit cells. For instance, a wideband DRA made up of four concentric rings with decreasing effective dielectric constants in the radial direction have been manufactured using the FDM technique [4]. 3D-printed homogeneous ceramic DRAs which effective permittivity is controlled by the printed lattice have also been proposed [5]. In the end, all these DRAs use engineered isotropic dielectrics whereas additive manufacturing may also allow to obtain anisotropic dielectrics that can provide an additional degree of freedom in the design of DRAs [6].

In this letter, we first discuss the engineering of dielectric anisotropy within 3D-printed ceramics. Such materials are then put to the test by the design of a single fed DRA in circular polarisation (CP) that relies on a 3D-printed uniaxial anisotropic ceramic.

Engineering the dielectric anisotropy of 3D-Printed ceramics: In order to obtain anisotropic dielectrics at microwave frequencies, one can use periodic structures made up of unit cells that do not exhibit rotational symmetry [7]. When the unit cell is kept sufficiently small compared to the wavelength, the resulting material can behave, for instance, as a uniaxial anisotropic dielectric which effective dielectric permittivity is given by

$$\bar{\bar{\varepsilon}} = \varepsilon_0 \begin{bmatrix} \varepsilon_x & 0 & 0 \\ 0 & \varepsilon_t & 0 \\ 0 & 0 & \varepsilon_t \end{bmatrix}. \quad (1)$$

Such periodic structures can be manufactured by 3-D-printing unit cells made up of both air and dielectric. One may note however that the strength of the anisotropy, or birefringence, defined as $\Delta\varepsilon = |\varepsilon_x - \varepsilon_t|$ remains limited when using low dielectric constant materials. Here, we propose to use the 3D-printer C900 FLEX from 3DCERAM that relies on SLA with a photosensitive paste compound containing zirconia powder [8]. In addition to the interesting mechanical properties of ceramics, the high dielectric constant $\varepsilon_r = 32.5$ and low dielectric loss tangent $\tan\delta = 0.002$ of zirconia make it a good candidate for manufacturing 3D-printed anisotropic dielectrics with large dielectric constants and birefringence.

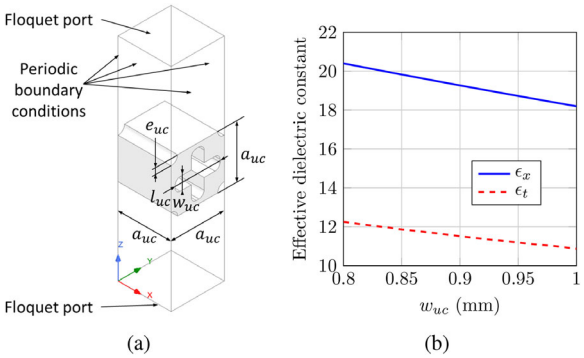

(a) (b)

Fig. 1 *(A) design of the proposed 3D-printed uniaxial anisotropic unit cell and (b) example of simulated effective permittivity tensor obtained as a function of w_{uc} at 2.45 GHz ($a_{uc} = 3.30$ mm, $l_{uc} = 2.80$ mm, and $e_{uc} = 0.40$ mm)*

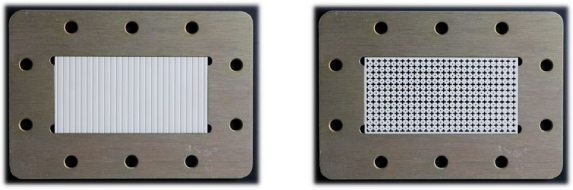

(a) (b)

Fig. 2 *Pictures of 3D-printed ceramic samples ($a_{uc} = 3.30$ mm, $l_{uc} = 2.80$ mm, $e_{uc} = 0.40$ mm and $w_{uc} = 0.84$ mm) within a WR340 sample holder to measure (a) ε_x and (b) ε_t values at 2.45 GHz*

The proposed subwavelength unit cell is described in Figure 1(a). It is made up of zirconia and air. Its anisotropy is due to the air holes placed along the x-direction that break its rotational symmetry, namely a cross-shaped in its centre and cylindrical holes on its sides. This design leads to uniaxial anisotropy since we have the same effective dielectric constant ε_t along y- and z-directions as in Equation (1). Finally, both ε_x and ε_t can be controlled by changing the air-filling ratio of the unit cell through the parameters l_{uc}, w_{uc}, and e_{uc}. Nevertheless, note that a minimum thickness of 0.5 mm for zirconia walls must be respected to satisfy the manufacturing constraints. This unit cell is simulated and optimised using periodic boundary conditions on Ansys HFSS, and its effective permittivity tensor is retrieved through the simulated S-parameters [9]. In order to find ε_x and ε_t, the incident electric field is successively polarised in x- and y-directions. Respecting manufacturing constraints, and assuming $a_{uc} = 3.30$ mm, a maximum birefringence $\Delta\varepsilon$ of 8 can be obtained, for instance, at the 2.45 GHZ ISM band as illustrated in Figure 1(b).

In order to validate the manufacturing process, a specific unit cell has been designed in simulation to obtain $\varepsilon_x = 20$ and $\varepsilon_t = 12$ at 2.45 GHz, i.e. a birefringence $\Delta\varepsilon = 8$. Its optimised dimensions are $a_{uc} = 3.30$ mm, $l_{uc} = 2.80$ mm, $e_{uc} = 0.40$ mm, and $w_{uc} = 0.84$ mm. Note that the unit cell size a_{uc} remains smaller than one eighth of the wavelength in the dielectric at 2.45 GHz for the largest value of the permittivity tensor, namely $\varepsilon_x = 20$. Two samples have been 3D-printed as shown in Figure 2(a,b) to measure ε_x and ε_t, respectively. Their thickness is equal to 5 mm, while their lateral dimensions are equal to 86.3 and 43.1 mm to fit in a WR340 rectangular waveguide. The samples were inserted into a waveguide section and measured separately. The Nicolson-Ross-Wier (NRW) method has been applied for parameter retrieval [10, 11]. We obtain $\varepsilon_x = 18.9$ and $\varepsilon_t = 11.5$ in measurements at 2.45 GHz, i.e. a maximum error of 5.5% and 4.1% for ε_x and ε_t, respectively. Those errors are within the manufacturing tolerances, namely the resolution of the 3D-printer, and the accuracy of the measurement technique [12].

In order to demonstrate the capability of 3D-printed anisotropic ceramics we propose to design, 3D-print, and measure a single-fed CP DRA which principle of operation relies on dielectric anisotropy.

Operating principle of the DRA example: A rectangular dielectric resonator (DR) is considered with dimensions a, b, and d along x-, y- and z-directions, respectively. The proposed single-fed CP DRA relies on the excitation of two orthogonal modes in phase quadrature inside this rectangular DR, namely the TE^x_{111} and TE^y_{111} modes in our case. To achieve CP at the centre frequency f_0, the resonant frequencies of both modes must satisfy the following conditions [13]

$$f_1 \approx f_0\left(1 - \frac{1}{2Q_1}\right) \tag{2}$$

and

$$f_2 \approx f_0\left(1 + \frac{1}{2Q_2}\right) \tag{3}$$

where f_1 and Q_1 are the resonant frequency and quality factor of the TE^y_{111} mode, while $f_2 > f_1$ and Q_2 refer to the TE^x_{111} mode. Practical implementations for having two modes respecting these criteria include, for example, rectangular shape DRA [14], or a square one with truncated corners [15]. Instead of modifying the DRA shape, we here consider a perfectly square DRA with $a = b$ for which modes are tuned by modifying the permittivity tensor of a uniaxial anisotropic dielectric medium as described by Equation (1) [16]. In that case, the TE^x_{111} mode remains as with an isotropic DR since the x-component of the electric field vanishes ($E_x = 0$) and the dielectric constants along y- and z-directions are both equal to ε_t. Applying the dielectric waveguide model (DWM), the resonant frequency f_2 and the quality factor Q_2 can easily be derived [17].

Regarding the properties of the TE^y_{111} mode, its resonant frequency f_1 is altered by the anisotropic properties of the DR. As derived in [18], it can be obtained from the transcendental equation

$$k_y \tan\left(\frac{k_y b}{2}\right) = \sqrt{k_x^2 + k_z^2 - k_1^2} \tag{4}$$

where $k_1 = (2\pi f_1)/c$ is the free-space wavenumber, c is the speed of light in vacuum, and k_y is calculated using the following equation

$$\frac{k_x^2}{k_1^2\varepsilon_t - k_y^2} + \frac{k_z^2}{k_1^2\varepsilon_x - k_y^2} = 1 \tag{5}$$

with $k_x = \pi/a$ and $k_z = \pi/d$.

The quality factor Q_1 is then given by [18]

$$Q_1 = \frac{\omega_1 \mu_o \pi^6}{640 k_1^6 abd} \frac{[1 + \mathrm{sinc}(k_y b)]}{\mathrm{sinc}(k_y b/2)^2} \frac{\left[\frac{\varepsilon_t k_x^2}{(k_1^2\varepsilon_t - k_y^2)^2} + \frac{\varepsilon_x k_z^2}{(k_1^2\varepsilon_x - k_y^2)^2}\right]}{\left[\frac{(\varepsilon_t - 1)k_x a}{k_1^2\varepsilon_t - k_y^2} + \frac{(\varepsilon_x - 1)k_z d}{k_1^2\varepsilon_x - k_y^2}\right]^2}. \tag{6}$$

Finally, to design the DR for achieving CP, we impose $b = a$ and we fix d, ε_t, and f_0. For finding a, we consider a list of discrete possible values, and for each of these values, we first find f_2, and then we determine Q_2 [17]. Finally, we choose the value of a for which f_2 and Q_2 best satisfy Equation (3). Similarly, by means of Equations (4)–(6), from a list of discrete possible values, we choose the value of ε_x for which f_1 and Q_1 best satisfy Equation (2).

The proposed methodology is applied to design a single-fed CP DRA for the 2.45 GHz ISM band. We first fix $d = 25.20$ mm, $\varepsilon_t = 12$, and $f_0 = 2.45$ GHz. In order to satisfy Equation (3), the DRA size must be $a = b = 27.60$ mm. Finally, the dielectric constant ε_x must be equal to 18 to satisfy Equation (2). We then obtain analytically $f_1 = 2.34$ GHz, $Q_1 = 12.5$, $f_2 = 2.58$ GHz, and $Q_2 = 9.6$. These results are verified with Ansys HFSS using an eigenmode analysis and perfectly matched layers (PML) as boundary conditions. A good agreement is achieved with $f_1 = 2.36$ GHz, $Q_1 = 12.7$, $f_2 = 2.59$ GHz, and $Q_2 = 10.1$.

Design of the DRA example: Figure 3(a) presents the exploded view of the single-fed CP DRA designed for the 2.45 GHz ISM band. Three solid walls of zirconia (in grey in Figure 3(a)) are added for mechanical reasons during 3D-printing, two laterals with 1 mm thickness and one around the coaxial probe with 0.5 mm thickness. As a result, a numerical optimisation is performed using Ansys HFSS to tune the DRA while taking into account the feeding coaxial probe, finite size ground plane, and solid dielectric walls. Note that the DR has been modelled including both a solid isotropic dielectric material for the walls (in grey in Figure 3(a)), and a solid anisotropic dielectric material for the core resonator

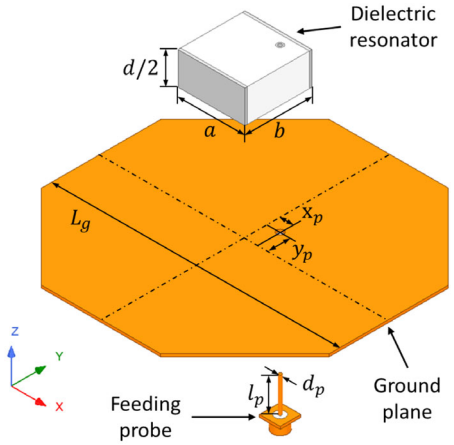

(a)

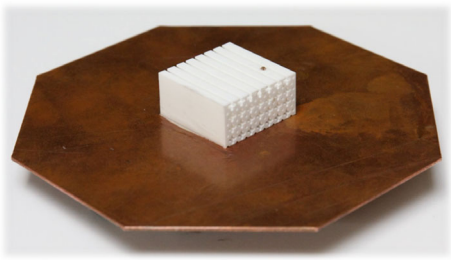

(b)

Fig. 3 *(A) exploded view of the uniaxial anisotropic DRA where the grey parts of the dielectric resonator represent the isotropic zirconia walls ($a = b = 25.80$ mm, $d = 25.20$ mm, $L_g = 110.87$ mm, $l_p = 12.60$ mm, $d_p = 1.23$ mm, $x_p = 5.29$ mm, and $y_p = 8.29$ mm) and (b) picture of the 3D-printed DRA*

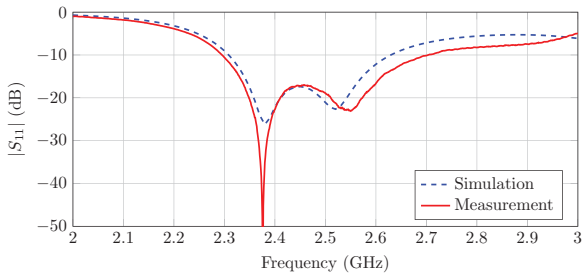

Fig. 4 *Simulated and measured reflection coefficients of the 3D-printed DRA*

(in white in Figure 3(a)). The position of the coaxial probe has been chosen to obtain left-hand circular polarisation (LHCP), but right-hand circular polarisation (RHCP) can also be achieved by changing the probe location. The final DRA dimensions are $a = b = 25.80$ mm and $d = 25.20$ mm, and its permittivity tensor in the anisotropic region is so that $\varepsilon_t = 12$ and $\varepsilon_x = 20$. Figure 3(b) presents a picture of the manufactured DRA. The dimensions of the realised 3D-printed DR are $a = 26.0$ mm, $b = 26.1$ mm, and $d = 25.5$ mm, i.e. a maximum error of 1.2% with respect to the original dimensions.

Simulated and measured results for the DRA example: The 3D-printed DRA of Figure 3(b) was measured with a Rohde and Schwarz ZVL-13 vector network analyser in the indoor far-field test range of ISAE-SUPAERO.

Figure 4 shows the simulated and measured reflection coefficients as a function of the frequency. We observe a good agreement between the numerical and experimental results. The measured 10 dB impedance bandwidth (i.e. $|S_{11}| \leq -10$ dB) is equal to 16% from 2.3 to 2.7 GHz.

Figure 5 shows the simulated and measured axial ratio (AR) as a function of the frequency at boresight ($\theta = 0^\circ$). We observe a slight difference in magnitude between the simulated and measured AR that is due to manufacturing tolerances during the 3D-printing process. The minimum value for the measured AR is obtained at 2.47 GHz with a 3 dB AR bandwidth of 2.4% from 2.44 to 2.5 GHz. We observe that the AR

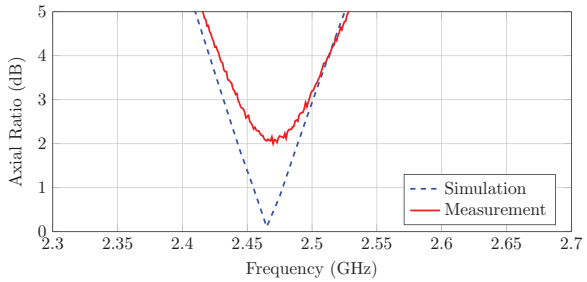

Fig. 5 *Simulated and measured axial ratios of the 3D-printed DRA considering* $\theta = 0°$ *and* $\phi = 0°$

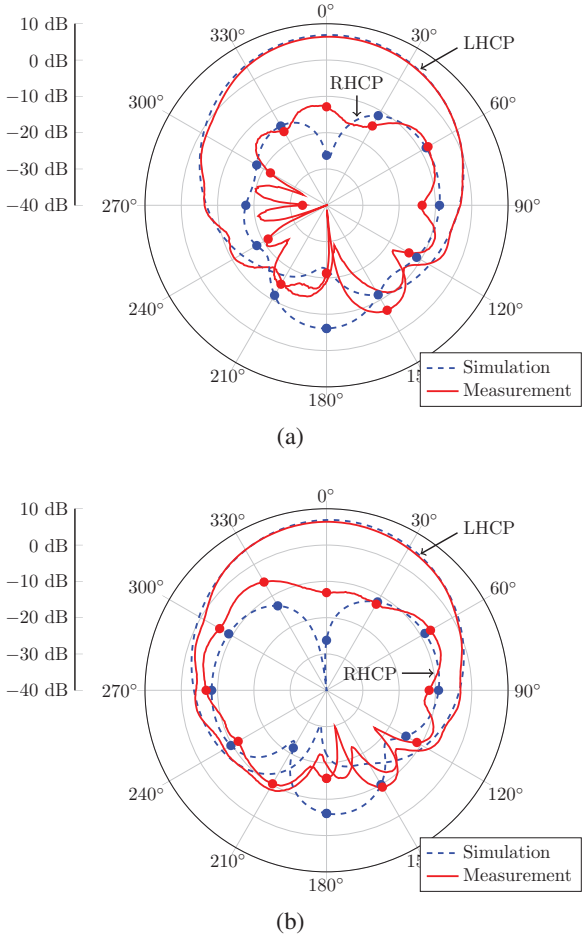

Fig. 6 *Simulated and measured realised gain of the 3D-printed DRA considering* $f = 2.47$ *GHz and (a)* $\phi = 0°$ *and (b)* $\phi = 90°$

bandwidth is much lower than the 10 dB impedance bandwidth. This difference is not due to the anisotropy of the dielectric resonator, but rather to the use of a single-fed CP DRA relying on the excitation of two orthogonal modes in phase quadrature as observed in [13, 14].

Finally, Figure 6 shows the simulated and measured realised gain patterns of the 3D-printed DRA at 2.47 GHz. We validate that the antenna is operating in LHCP. Once again, a good agreement is obtained between measurement and simulations. The measured realised gain at boresight and simulated radiation efficiency are equal to 6.4 dBi and 97%, respectively, at 2.47 GHz.

Conclusion: 3D-printed ceramics with engineered dielectric anisotropy have been presented. More specifically, their permittivity tensor has been controlled by 3D-printing a periodic structure of subwavelength cubic unit cells that do not exhibit rotational symmetry. A sample has been designed and 3D-printed by controlling the filling ratio of zirconia and air in its unit cells. It finally exhibits uniaxial dielectric anisotropy with a large birefringence of 7.4.

To demonstrate the use of 3D-printed anisotropic ceramics for DRA applications, a single-fed DRA in LHCP has been designed in the 2.45 GHz ISM band. Its principle of operation relies on the excitation of two orthogonal modes which magnitudes and phase difference have been tuned by modifying the anisotropy of the DR. A reasonable agreement has been observed between simulated and measured results. This DRA has a measured 10 dB impedance bandwidth of 16%, a 3 dB AR bandwidth of 2.4%, and a 6.4 dBi realised gain at 2.47 GHz.

Finally, the use of 3D-printed anisotropic ceramics could open up interesting perspectives in the design of new dielectric-based antennas.

Acknowledgments: The authors would like to thank C. Cailhol of ISAE-SUPAERO for his help with measurements. The authors would also like to thank the Région Occitanie and ENAC for their financial support.

Received: *16 April 2021* Accepted: *11 May 2021*
doi: 10.1049/ell2.12234

References

1 Petosa, A., Ittipiboon, A.: Dielectric resonator antennas: A historical review and the current state of the art. *IEEE Antennas Propag. Mag.* **52**(5), 91–116 (2010)
2 Basile, V., et al.: Design and manufacturing of super-shaped dielectric resonator antennas for 5G applications using stereolithography. *IEEE Access* **8**, 82929–82937 (2020)
3 Zhang, S.: Three-dimensional printed millimetre wave dielectric resonator reflectarray. *IET Microw. Antennas Propag.* **11**(14), 2005–2009 (2017)
4 Xia, Z.-X., Leung, K.W., Lu, K.: 3-D-printed wideband multi-ring dielectric resonator antenna. *IEEE Antennas Wirel. Propag. Lett.* **18**(10), 2110–2114 (2019)
5 Thevenot, M., et al.: A dielectric resonator antenna designed with a structured dielectric material. In: Proc. of IEEE Conf. on Antenna Measurements and Applications, pp. 1–2.IEEE, Piscataway, NJ (2018)
6 Fakhte, S., Oraizi, H., Matekovits, L.: High gain rectangular dielectric resonator antenna using uniaxial material at fundamental mode. *IEEE Trans. Antennas Propag.* **65**(1), 342–347 (2017)
7 Rumpf, R.C.: Engineering the dispersion and anisotropy of periodic electromagnetic structures. *Solid State Physics* **66**, 213–300 (2015)
8 Doreau, F., Chaput, C., Chartier, T.: Stereolithography for manufacturing ceramic parts. *Adv. Eng. Mater.* **2**(8), 493–496 (2000)
9 Numan, A.B., Sharawi, M.S.: Extraction of material parameters for metamaterials using a full-wave simulator. *IEEE Antennas Propag. Mag.* **55**(5), 202–211 (2013)
10 Nicolson, A.M., Ross, G.F.: Measurement of the intrinsic properties of materials by time-domain techniques. *IEEE Trans. Instrum. Meas.* **19**(4), 377–382 (1970)
11 Weir, W.B.: Automatic measurement of complex dielectric constant and permeability at microwave frequencies. *Proc. IEEE* **62**(1), 33–36 (1974)
12 Deffenbaugh, P.I., Rumpf, R.C., Church, K.H.: Broadband microwave frequency characterization of 3-D printed materials. *IEEE Trans. Compon. Packag. Manuf. Technol.* **3**(12), 2147–2155 (2013)
13 Langston, W.L., Jackson, D.R.: Impedance, axial-ratio, and receive-power bandwidths of microstrip antennas. *IEEE Trans. Antennas Propag.* **52**(10), 2769–2774 (2004)
14 Oliver,et al.: Circularly polarised rectangular dielectric resonator antenna. *Electron. Lett.* **31**(6), 418–419 (1995)
15 Haneishi, M., Takazawa, H.: Broadband circularly polarised planar array composed of a pair of dielectric resonator antennas. *Electron. Lett.* **21**(10), 437–438 (1985)
16 Morales, C.D., et al.: Single-fed circularly polarized dielectric resonator antenna using a uniaxial anisotropic material. In: IET Antennas and Propagation Conference, pp. 1–5.IET, Stevenage (2019)
17 Mongia, R.K., Ittipiboon, A.: Theoretical and experimental investigations on rectangular dielectric resonator antennas. *IEEE Trans. Antennas Propag.* **45**(9), 1348–1356 (1997)
18 Fakhte, S., Oraizi, H.: Analysis and design of rectangular uniaxial and biaxial anisotropic dielectric resonator antennas. *Prog. Electromagn. Res. C* **62**, 43–50 (2016)